Monthly Notices of the ROYAL ASTRONOMICAL SOCIETY

MNRAS **476,** 1371–1383 (2018) doi:10.1093/mnras/sty313
Advance Access publication 2018 February 9

The evolution of grain mantles and silicate dust growth at high redshift

Cecilia Ceccarelli,[1,2★] Serena Viti,[3★] Nadia Balucani[1,2,4★] and Vianney Taquet[2]

[1]*IPAG, Université Grenoble Alpes, CNRS, F-38000 Grenoble, France*
[2]*INAF-Osservatorio Astrofisico di Arcetri, Largo E. Fermi 5, I-50125 Florence, Italy*
[3]*Department of Physics and Astronomy, University College London, Gower St., London WC1E 6BT, UK*
[4]*Dipartimento di Chimica, Biologia e Biotecnologie, Via Elce di Sotto, 8, I-06123 Perugia, Italy*

Accepted 2018 January 31. Received 2018 January 22; in original form 2017 December 8

ABSTRACT

In dense molecular clouds, interstellar grains are covered by mantles of iced molecules. The formation of the grain mantles has two important consequences: it removes species from the gas phase and promotes the synthesis of new molecules on the grain surfaces. The composition of the mantle is a strong function of the environment that the cloud belongs to. Therefore, clouds in high-zeta galaxies, where conditions – like temperature, metallicity, and cosmic ray flux – are different from those in the Milky Way, will have different grain mantles. In the last years, several authors have suggested that silicate grains might grow by accretion of silicon-bearing species on smaller seeds. This would occur simultaneously with the formation of the iced mantles and be greatly affected by its composition as a function of time. In this work, we present a numerical study of the grain mantle formation in high-zeta galaxies, and we quantitatively address the possibility of silicate growth. We find that the mantle thickness decreases with increasing redshift, from about 120 to 20 layers for z varying from 0 to 8. Furthermore, the mantle composition is also a strong function of the cloud redshift, with the relative importance of CO, CO_2, ammonia, methane, and methanol highly varying with z. Finally, being Si-bearing species always a very minor component of the mantle, the formation of silicates in molecular clouds is practically impossible.

Key words: astrochemistry – dust, extinction – ISM: molecules – galaxies: high-redshift – galaxies: ISM.

1 INTRODUCTION

As it is well known, the interstellar medium (ISM) is made up of gas and dust, the latter composed of silicates and carbonaceous material (Hoyle & Wickramasinghe 1969; Jones et al. 2013, 2017). In recent years, a heated debate has arisen on the quantity of silicates in the high-redshift ISM and on its formation (Draine 2009; Michalowski et al. 2010; Mancini et al. 2015; Zhuvkovska et al. 2016; Ginolfi et al. 2018). In the local ISM, the major sources of silicates are believed to be the asymptotic giant branch (AGB) stars and, to a lesser extent, supernovae (SNe), although large uncertainties exist about how much dust is formed in both cases (e.g. Sugerman et al. 2006; Barlow et al. 2010; Nanni et al. 2013; Ventura et al. 2014; De Looze et al. 2017). At high redshifts, the situation is less clear, as low-mass stars, in principle, do not have time to evolve into AGBs (but see Valiante et al. 2009, 2011). Therefore, some authors have argued that the major source of high-z silicates is SNe (Kozasa, Hasegawa & Nomoto 1991; Todini & Ferrara 2001; Schneider, Ferrara & Salvaterra 2004; Bianchi & Schneider 2007; Dwek, Galliano & Jones 2007). Alternatively, others claim that silicates might grow, meaning that they form, and not only coagulate from smaller grains, in the cold and dense molecular clouds, via the freeze-out of atomic silicon or SiO molecules (e.g. Valiante et al. 2011; Asano et al. 2013; Hirashita & Voshchinnikov 2014; Mancini et al. 2015; Ginolfi et al. 2018). All these studies implicitly assume that gaseous Si and SiO would accrete into small silicate seeds, which can then grow. However, there are two difficulties with this assumption.

First, the formation of silicates is unlikely to occur in cold environments (e.g. Goumans & Bromley 2012). Several laboratory experiments show that SiO easily dimerizes, even at low temperatures, if a seed of TiO_2 or silicates are already present. SiO molecules can also form clusters that can eventually condense as solid silicon oxide (see e.g. Krasnokutski et al. 2014 and references there). However, neither SiO dimers nor clusters form 'real' silicates. Besides, SiO dimers or clusters do not have the correct silicon/oxygen ratio to become silica (based on SiO_2 crystals) or silicate (SiO_4 crystals). The second difficulty in the 'Si, SiO freeze-out = silicate growth' scheme is the following. Even if, via some unknown process, the formation of silicate occurs in cold environments, it is unlikely that the accreted Si or SiO will meet on the surface and form the necessary dimers or clusters. In a recent study, Ferrara, Viti & Ceccarelli (2016) analytically argued that, at a redshift of ~ 6, SiO molecules

★ E-mail: cecilia.ceccarelli@univ-grenoble-alpes.fr (CC); sv@star.ucl.ac.uk (SV); nadia.balucani@unipg.it (NB)

will be prevented from getting in contact with the silicate surface and from forming silicate-like bonds because of the formation of icy mantles, but no specific modelling was carried out.

While we cannot say more than what is already known about the silicate formation from a chemical point of view (which is summarized above), we can compute the probability that two or more Si and SiO species meet on the grain surface to form dimers or clusters. Whether they would then build up a silicate-like bond remains speculative at this point. None the less, it is first important to assess whether there is a non-zero probability to have dimers and clusters in the first place. In practice, the formation of Si or SiO dimers and clusters might only occur in the cold molecular clouds (see Ferrara et al. 2016), when the grain mantles form. The question is then what is the abundance of Si and SiO on each layer of the mantle with respect to other mantle species. If, for example, in one layer we have 1/100 SiO molecules with respect to the other frozen molecules, the probability that two SiO are close enough to form a dimer is 10^{-2} and even less for a SiO cluster. Therefore, the possible grain growth is closely connected with the formation of the grain iced mantle process.

ISO, *Akari*, and *Spitzer* satellites have provided us with a plethora of NIR observations on the composition of dust ices towards Galactic star-forming regions and a few external nearby galaxies. These observations show that the interstellar grain mantles are prevalently made of water ice, with a smaller fraction of CO, CO_2, CH_4, NH_3, and CH_3OH, at a level of 5–30 per cent each (Boogert, Gerakines & Whittet 2015, and references therein). The current explanation for the relatively high abundance of these iced species (when compared to their gas-phase abundances) is that hydrogenation and, possibly, oxidation of atoms (C, O, and N) and simple molecules (CO) take place on the grain surfaces. For example, water is believed to be the result of hydrogenation of the oxygen atoms landing on the grain surfaces (Dulieu et al. 2010; Lamberts et al. 2014), while formaldehyde and methanol are the hydrogenated products of CO (e.g. Watanabe & Kouchi 2002; Rimola et al. 2014; Song & Kastner 2017).

In addition to having a crucial role in the possible grain growth, the icy mantle formation heavily influences the chemical and physical evolution of the gas and dust in the clouds, because reactants and coolants are removed from and then re-injected into the gas phase. In turn, the icy mantle formation depends on a complicated time-dependent, non-linear chemistry highly affected by the physical environment. While several theoretical studies have concentrated on exploring how the gas chemical composition may vary with the different physical conditions that characterize the ISM of external galaxies, such as metallicity, gas density, cosmic ray (CR) ionization rate, and far-UV radiation intensity (e.g. Bayet et al. 2009, 2011; Meijerink et al. 2011; Bisbas, Papadopoulos & Viti 2015; Acharyya & Herbst 2016), no theoretical study on how ices change with such parameters has been carried out so far.

With this paper, we aim to fill up this gap. Its focus is the study of the formation of the grain iced mantles at high redshift z, with the twofold scope to understand how they change with z and to quantify the probability that SiO dimers or clusters form and, eventually, grow into silicates. To this end, we revise the chemical reactions involving Si-bearing species that can occur on the grain surfaces and model the evolution of ices as a function of several physical parameters that, as a function of redshift, are likely to differ from galactic values (Section 2). We then explore the abundances of the main ice components as well as Si-bearing solid species in order to quantify whether grain growth at high redshift can indeed be efficient enough to account for the potential missing dust mass (Section 3). Finally, in Section 5, we comment on the implications of our study.

Table 1. Top half: list of reactions occurring on the grain surfaces involving the oxidation of SiO. The last column reports the value of the energy barrier in K, as computed by Martin, Blitz & Plane (2009). Lower half: binding energies of the Si-bearing species considered in this study, as measured by He, Acharyya & Vidali (2016b).

No.	Reactants		Products	E_{act} (K)
1	Si + O	→	SiO	0
2	SiO + O	→	SiO_2	1000
3	SiO + OH	→	SiO_2 + H	0

Species	E_b (K)
Si	2700
SiO	3500
SiO_2	4300

2 CHEMICAL MODELLING

The code that we use in this study is based on the GRAINOBLE model (Taquet, Ceccarelli & Kahane 2012; Taquet et al. 2013). It is a time-dependent grain–gas chemistry code that also allows us to follow the structure of the layered grain mantles as a function of time. The code used here adopts the formalism by Hasegawa & Herbst (1993) for computing the surface reactions, keeping the layered structure composition (Taquet, Charnley & Sipila 2014). Briefly, the code computes the abundance of grain surface and gas-phase species as a function of time. In the following, we give a short summary of the processes included in the code, the updated chemical network that we use for this study, and describe the parameters of the modelled cloud.

2.1 Processes

Accretion: Species can accrete from the gas to the grain surfaces at a rate k_{accr}, following the standard formalism:

$$k_{accr} = S_x \pi a^2 n_{grain} v_x, \quad (1)$$

where S_x is the sticking probability of the accreting species x, a the (average) grain radius, n_{grain} the grain number density, and v_x the velocity of the gaseous species x with mass m_x and kinetic temperature T_{gas} [$v_x = (2k_B T_{gas}/m_x)^{1/2}$, where k_B is the Boltzmann constant]. Following the experimental study by He, Acharyya & Vidali (2016a), we assumed that the sticking coefficient S_x is equal to unity for all species except atomic hydrogen, for which we followed the formalism in Tielens (2005).

Diffusion: Once on the grain surface, the species can diffuse via the standard thermal hopping process. The diffusion energy is assumed to be 0.5 times the binding energy E_b of the species. The binding energies are listed in Taquet et al. (2012, 2014) and are updated according to He et al. (2016b). For Si, SiO, and SiO_2, the main species of interest in this work, we give the adopted value of their binding energies in Table 1.

Surface reactions: Species on the grain surfaces can meet, react, and form other species, following the Langmuir–Hinshelwood mechanism. The reaction rate is given by the product of the diffusion rate (see above) and the probability of the reaction. For radical–radical reactions, the latter is equal to unity; otherwise, it is a function of the reaction energy barrier E_{act} and it is calculated following the Eckart model (see Taquet et al. 2013 for more details).

Note that H-tunnelling can make the reaction efficient, despite the presence of a barrier (e.g. Rimola et al. 2014). GRAINOBLE considers that the reaction can only occur on the species within the last two mantle layers (i.e. the surface), namely the bulk of the mantle is assumed chemically inert.

Desorption: Species on the grain surfaces can be injected into the gas phase via thermal desorption, CR-induced desorption, and chemical desorption, in each case following the relevant standard formalism (e.g. Taquet et al. 2012). The first two desorption mechanisms depend on the species binding energy (see above), while for the latter we assumed that 1 per cent of species formed on the grain surfaces are injected back into the gas phase (Garrod, Wakelam & Herbst 2007).

Gas-phase reactions: Species in the gas undergo two-body reactions as the three-body reactions are extremely rare at the considered densities.

2.2 Chemical networks

For the reactions occurring in the gas phase, we used the KIDA 2014 network (Wakelam et al. 2015 , http://kida.obs.u-bordeaux1.fr), updated with the reactions described in Loison et al. (2014), Balucani, Ceccarelli & Taquet (2015), and Skouteris et al. (2017).

The reactions on the grain surfaces leading to formaldehyde, methanol, and water are described in Taquet et al. (2013) and Rimola et al. (2014). In addition, we inserted the hydrogenation of C, N, and Si atoms, which has no energy barrier and leads respectively to methane (CH_4), ammonia (NH_3), and silane (SiH_4, and the respective partially hydrogenated species).[1]

Finally, in the grain surface reaction network, we included the oxidation of Si and SiO, which leads to SiO and SiO_2, respectively. The first reaction, Si + O → SiO, is barrierless. For the oxidation of SiO, we considered the reactions with O and OH. The first one has a large barrier, whereas the second reaction is barrierless (contrarily to the CO + OH reaction) and has a rate of 6×10^{-12} cm^{-3} s^{-1} (Martin et al. 2009). Table 1 summarizes the SiO oxidation reactions and the binding energies E_b of the Si-bearing species considered in this study.

2.3 Cloud temperature, elemental abundances, and other parameters

We model a molecular cloud in a galaxy at a given redshift z. We assume that the cloud is completely shielded from the UV photons of the interstellar radiation field and that the H number density of the molecular cloud, n_H, is constant and equal to 2×10^4 cm^{-3}. In the simulations, we assume an average grain radius of 0.1 μm,[2] typical of the galactic ISM grains (e.g. Jones et al. 2013).

The dust and gas are assumed to be thermally coupled, which, at the considered density and conditions, is approximately correct (e.g. Goldsmith 2001; Gong, Ostriker & Wolfire 2017). The temperature is constant with time and depends on the redshift of the molecular cloud. Specifically, we assumed that the cloud temperature is ∼10 K larger than the cosmic microwave background (CMB) temperature at a given redshift to account for the additional dust heating from the interstellar photon field (Table 3). We note that ∼10–12 K are the average gas and dust temperatures in galactic molecular clouds.

Table 2. List of the gaseous elemental abundances, with respect to H nuclei, used in the simulations. Column 'Ref.' lists the abundances of our reference model. Columns '*met*0.1' and '*met*0.01' refer to metallicities 0.1 and 0.01 with respect to the solar one, namely all species are scaled by that factor (see the text for details). Column 'Cosmo' lists the abundances as derived by cosmological simulations (see the text).

Element	Unit	Abundance wrt H			
		Ref.	*met*0.1	*met*0.01	Cosmo
H	1	1	1	1	1
He	1	0.85	0.85	0.85	0.92
O	($\times 10^{-4}$)	2.5	0.25	0.025	1.8
C	($\times 10^{-4}$)	1.3	0.13	0.013	0.55
N	($\times 10^{-5}$)	6.8	0.68	0.068	2×10^{-6}
Cl	($\times 10^{-7}$)	1.5	0.15	0.015	0.02
F	($\times 10^{-7}$)	2.0	0.20	0.020	5×10^{-7}
Fe	($\times 10^{-7}$)	3.5	0.35	0.035	2.5
Mg	($\times 10^{-7}$)	4.0	0.40	0.040	6.5
Na	($\times 10^{-8}$)	1.2	0.12	0.012	0.97
P	($\times 10^{-7}$)	2.6	0.26	0.026	0.065
S	($\times 10^{-5}$)	1.3	0.13	0.013	0.03
Si	($\times 10^{-7}$)	3.2[a]	0.32	0.032	32

Notes. [a]The elemental Si abundance is a parameter varied in the simulations, as reported in Table 3.

The abundances of the elements in the gas phase are assumed to be the solar ones with the following modifications: (1) oxygen and carbon are assumed to be half on the refractory grains and half in the gas; (2) 90 per cent of chlorine is assumed to be depleted while 10 per cent is in the gas phase (which may be a pessimistic assumption, as Cl is not in rocky materials; see e.g. the discussion in Codella et al. 2012); (3) F, P, Fe, Mg, Al, Ca, and Na are largely depleted in the refractory grains and only 1 per cent is in the gas phase; (4) Si is a parameter of this study and we varied it from 90 per cent to 1 per cent of it being in the gas phase, in order to verify whether silicates can grow in molecular clouds. Table 2 summarizes the adopted elemental abundances.

The final mantle chemical composition depends also on two additional parameters: the cloud metallicity, *met*, and the CR ionization rate, ζ_{CR}. Thus, we explored a range of metallicity from 0.01 to 1 the solar one by reducing the elemental abundances by the same factor. We also consider a case where the elemental abundances are taken from simulations of the ISM enrichment from Pop III stars (see Table 2 and Section 3.3). Finally, CR ionization rate is governed by the rate of SN explosions (e.g. Morlino 2017), which might be a function of the redshift. Therefore, we run models covering the range 1×10^{-17} s^{-1}, equivalent to a low value in the Milky Way (Padovani, Galli & Glassgold 2009), to 1×10^{-14} s^{-1}, corresponding to a cloud irradiated by a 1000 times more intense CR flux (Vaupré et al. 2014), which might simulate the conditions in early galaxies.

Table 3 summarizes the parameters used in our simulations and the adopted values.

2.4 Chemical evolution

We started with a partially atomic cloud, meaning that all elements are in the atomic form (neutral or ionized depending on their ionization potential) except hydrogen, which is assumed to be in molecular form. This mimics the pseudo-evolution of a cloud from neutral to

[1] In the absence of specific quantum-chemistry computations or laboratory experiments, we assumed that the back reactions, like for example CH_2 + H → CH + H_2, do not take place, so that the final hydrogenated products might be slightly overestimated.

[2] Note that very small grains, ≤0.02 μm, are stochastically photon heated and the mantles do not survive (e.g. Hollenbach et al. 2009).

Table 3. Parameters varied in the simulations. We considered values aimed to simulate the conditions of clouds at redshifts 0, 3, 6, and 8, quoted in the first row, which correspond to the (dust and gas) temperatures of the second row. The temperature was computed by adding ∼10 K to the CMB one at a given redshift z and, specifically, varies from 10 to 35 K (see the text). The CR ionization rate ζ_{CR} varies from the Milky Way low value, 1×10^{-17} s^{-1}, to 1000 times larger, likely appropriate for early galaxies. The metallicity *met* varies from 0.01 to 1 of the elemental abundances listed in Table 2, to simulate different enrichment. In addition, we run a case with elemental abundances predicted by cosmological simulations, model Cosmo (see the text). Finally, the elemental silicon abundance in the gas phase, Si_{gas}, varies from 90 per cent (namely 2.9×10^{-5}) to 1 per cent (3.2×10^{-7}) of the solar value, to explore whether silicates can grow in molecular clouds. The values in boldface font refer to our reference model (see the text). The last column reports the number of each model, used in Table 4.

Parameter	Range of values	Model number
z	0, 3, **6**, 8	
Temperature (K)	10, 20, **30**, 35	1–4
ζ_{CR} ($\times 10^{-17}$ s^{-1})	**1**, 10, 100, 1000	5–8
met	Cosmo, 0.01, 0.1, **1**	9–12
Si_{gas}/Si_{sol}	**0.01** 0.1, 0.3, 0.9	13–16

molecular. The chemical composition of the cloud is left to evolve with time for 10 Myr. Note that GRAINOBLE follows the chemical evolution of each grain mantle layer, so that it provides the composition of each layer as the mantle grows. In general, the mantle is formed of about 100 layers, the exact number depending on the temperature, the CR ionization rate, and the elemental abundances (especially O, C, and N) assumed in the model (see the next section).

3 RESULTS

In this section, we shall investigate the composition of each layer of the icy mantles, for a comprehensive parameter space. To this scope, all the figures shall plot the fractional abundance (with respect to the total number of H nuclei) of selected frozen species as a function of time. Plots are reported for three sets of frozen species. The first set is formed by the major constituents of the grain mantles: H_2O, CO, CO_2, CH_4, and NH_3. The second set plots minor frozen species: CH_4, CH_3, H_2CO, and OH. Finally, the third set is focused on the Si-bearing frozen species, for assessing the possibility of silicate growth: SiO_2, SiO, SiH_4, and Si.

In order to evaluate whether grain growth can occur, it is important to show the ice evolution as a function of the building up of the layers. Note that for Si-bearing species to be able to form bonds on the core grain and, therefore, possibly form silicate-like bonds (see the introduction), they would have to be abundant in the first few layers. One can also think of a situation where small clusters of Si and SiO or SiO dimers can form in deeper layers and then they remain clustered when the mantles sublimate and, therefore, constitute small silicate seeds. In this case, in order to grow silicates, frozen Si and SiO have to be abundant and close to each other.

In the following, we will discuss separately the effects due to the different parameters.

3.1 The effect of the CMB temperature

In this section, we investigate the effect of increasing the CMB temperature on the icy mantle composition. We assumed that the cloud temperature is about 10 K larger than the CMB blackbody spectrum temperature, namely $T_{CMB} = T_0(1+z)$, with $T_0 = 2.725$ K.

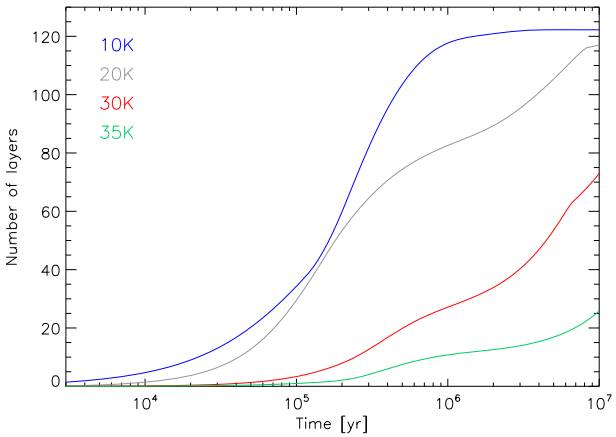

Figure 1. Number of layers of the grain mantle as a function of time for the four models with different cloud temperatures: 10 K (blue), 20 K (grey), 30 K (red: this is the reference model), and 35 K (green).

We, therefore, considered 10, 20, 30, and 35 K to simulate the clouds at z equal to 0, 3, 6, and 8 (Table 3).

Fig. 1 shows the number of layers composing the grain mantle as a function of time and for the different temperatures. Already from this figure it is clear that the temperature, namely the redshift of the cloud, has a great influence on the grain mantle growth: the larger the temperature, the smaller the number of mantle layers.

In order to understand how the redshift specifically affects the mantle composition, we first start with a quick analysis of the grain mantle composition of a 'standard' Milky Way cloud, namely a cloud with a temperature of 10 K (Figs 2–4). The mantle is composed of about 120 layers that grow in about 2–10$\times$ 10^5 yr (Fig. 1). The first layers are mostly composed of the hydrogenated forms of C and N, namely methane and ammonia. This is because our model starts with an atomic cloud, and when the C and N atoms land on the grain, they undergo hydrogenation, which is a fast process since it does not have energy barriers. After $\sim 10^5$ yr, the gaseous abundance of both C and N drops, as CO and N_2 form. On the other hand, the hydrogenation of oxygen takes more time than that of C and N because of the larger binding energy of O ($\sim$1400 K against $\sim$800 K of C and N; e.g. Bergeron et al. 2008). In addition, at early times ($\leq 10^5$ yr), atomic oxygen is more abundant than atomic hydrogen while iced CO starts to increase, so that the formation of iced CO_2 occurs before that of water (which is not a simple barrierless process). The first 35 mantle layers are, therefore, mostly constituted of ammonia, methane, and CO_2. Between about 1 and 3 $\times$ 10^5 yr, the abundances of atomic oxygen and hydrogen become comparable, and water formation takes over. The intermediate mantle layers are, therefore, dominated by water molecules. Finally, at $\geq 4 \times 10^5$ yr, the gaseous CO freezes out into the mantles and methanol is efficiently formed by its hydrogenation. The last 35 or so layers are a mix of water, CO, and methanol. Atomic Si and SiO are the major frozen Si-bearing species in the 35 layers closest to the bare surface of the grains, while starting from $\sim 10^5$ yr frozen silane and SiO equally dominate. Note that SiO_2 is never an important mantle component, being always at abundances lower than about 10^{-9}. We discuss later the implications for the possible silicate growth.

A first important effect caused by the increase of the CMB temperature and, consequently, the cloud temperature is that the mantle growth is slower and the mantles become thinner (Fig. 1). At 10^7 yr, while at 10 K the grain mantles have 122 layers, at 30 K they have 73. Indeed, the increased dust temperature has two effects: (1) the

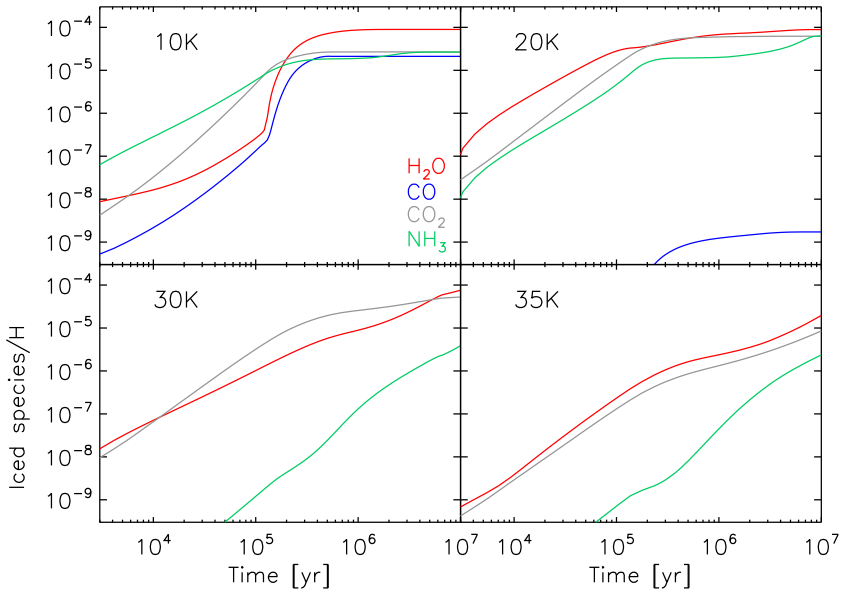

Figure 2. Grain mantle chemical structure. Cumulative fractional abundances with respect to the total number of hydrogen nuclei of iced water (red), CO (blue), CO_2 (grey), and ammonia (green) as a function of time. The cloud temperature is 10 K (upper-left panel), 20 K (upper-right panel), 30 K ((bottom-left panel), and 35 K (bottom-right panel).

residence times of H and O atoms, as well as of CO molecules, are shorter with increasing temperature so that the hydrogenation and oxidation processes are reduced; (2) when the dust temperature becomes larger than their sublimation temperatures (linked to their relative binding energies), CO and CH_4 cannot remain frozen on the surfaces. In summary, as the temperature increases, less and less molecules remain on the grain mantles and the mantle thickness, consequently, diminishes.

Also the composition dramatically changes with increasing CMB temperature. This is shown in Figs 2–4. We first discuss the major components of the mantle (Figs 2 and 3). Although water is always the major mantle component, the contribution of frozen CO_2 increases with increasing temperature (because of the non-residence of CO). Frozen CO and CH_4 disappear from the mantle for temperatures higher than 20–30 K, because of their relatively low binding energies. Frozen methanol is very abundant in the top mantle layers at temperatures $\leq$20 K, but at $\geq$30 K very little methanol is synthesized on the grain mantles. Finally, frozen ammonia decreases with increasing temperature, after a peak at 20 K, because of the balance of H-atom diffusion/residence time.

The abundances of Si-bearing molecules trapped into the grain mantles are shown in Fig. 4. In all cases, SiO is the major reservoir of frozen silicon, followed by silane. Silane, a frozen species so far not predicted by models, is as abundant as iced SiO for temperatures $\leq$20 K, and about four times less abundant at higher temperatures. Frozen atomic Si is present in appreciable quantities only at 10 K, since its oxidation and hydrogenation become more efficient with increasing temperature. Finally, SiO_2 only traps a very small fraction of frozen silicon.

In order to answer the question whether silicates can grow in molecular clouds, we need to focus on SiO, which might form dimers and clusters (see the introduction). Specifically, we need to quantify the probability to have one or more adjacent SiO molecules. Fig. 5 shows the abundance ratio of frozen SiO over the total number of frozen species on each layer forming the mantle, for the four cases with different CMB temperatures. We consider this ratio as the probability of two SiO molecules to be adjacent: it is larger than 10^{-2} only in the first few layers at a cloud temperature of 35 K. To quantify how many SiO dimers are statistically present in the mantle, we first plot the iced SiO abundance with respect to the total number of H nuclei in each layer (Fig. 5) and then multiplying it by the probability that two SiO molecules are adjacent: this gives the number of iced SiO dimers in the mantle in each layer. Fig. 5 shows this value normalized to the elemental silicon in the gas phase. Clearly, the number of possible iced SiO dimers is very small, always lower than 0.04 the gaseous available silicon. The most favourable case is for a cloud at 35 K and in the first $\sim$10 layers of the mantle. At lower temperatures, no more than $\sim$0.1 per cent of elemental silicon is frozen into SiO dimers. In addition, these dimers are more distant from the bare silicate surfaces with diminishing cloud temperature.

3.2 The effect of CR ionization rate

Theoretical sensitivity studies of the ISM gas-phase evolution have shown that several molecular species are very sensitive to the CR ionization rate ζ_{CR} (e.g. Bayet et al. 2011; Ceccarelli et al. 2011; Meijerink et al. 2011; Bisbas et al. 2015). In this section, we explore the response of the mantle composition to changes in ζ_{CR} of our reference model (Table 3). We select a range of ζ_{CR} intended to cover values likely appropriate for external galaxies. As CR are prevalently accelerated by SN explosions (e.g. Morlino 2017), the CR ionization rate is related to the formation rate of massive stars, and so it is large in active and early galaxies. Therefore, we varied ζ_{CR} from the conservative value for our Milky Way (1×10^{-17} s^{-1}) up to 1000 times larger (1×10^{-14} s^{-1}), a value that has been invoked for the Ultra Luminous Infra Red Galaxy Arp 220 (Bayet et al. 2011).

Figs 6–8 show the results of these simulations. First, the number of layers increases from 73 (reference model: see above) to 100, 111, and 112 for ζ_{CR} equal to 10, 100, and 1000 times the standard value of 10^{-17} s^{-1}. Indeed, increasing ζ_{CR} leads to an increase in the water ice abundance as the abundance of atomic O increases because of destruction of CO in the gas by the CR. While frozen

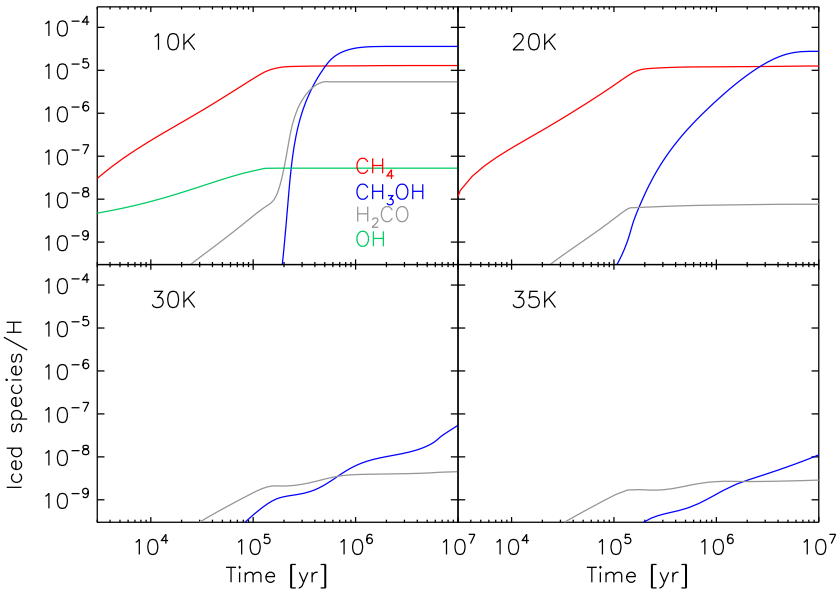

Figure 3. As Fig. 2 for iced methane (red), methanol (blue), formaldehyde (grey), and OH (green).

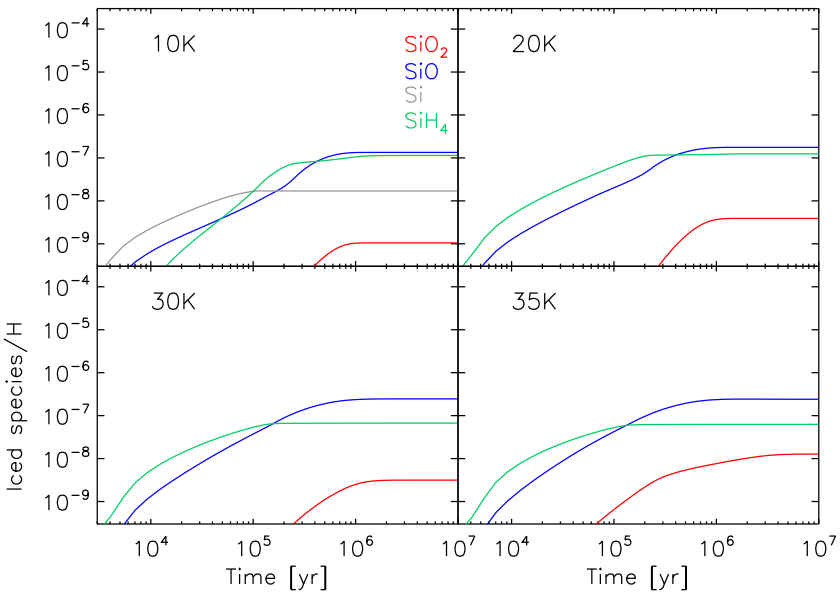

Figure 4. As Fig. 2 for iced SiO_2 (red), SiO (blue), atomic Si (grey), and silane (green).

water increases, CO_2 diminishes with increasing cloud temperature. At $\zeta \geq 10^{-16}$ s^{-1} water dominates over CO_2 ice and the iced CO_2 abundance gradually drops from $\sim 10^{-4}$ to $\sim 10^{-7}$ at large ζ (Fig. 6). Similarly, methanol and formaldehyde (not shown), the other mantle components of the reference model (Fig. 3), disappear from the mantles with increasing ζ as CO is destroyed in the gas by the CR.

Increasing the CR ionization rate causes the disappearance of SiO_2 from the mantles at $\zeta \geq 10^{-15}$ s^{-1} and that of SiO at $\zeta \geq 10^{-14}$ s^{-1}. Starting from $\zeta \sim 10^{-15}$ s^{-1}, silane becomes the major reservoir of iced silicon (Fig. 4).

The ratio of frozen SiO over the total frozen species diminishes with increasing ζ_{CR} (Fig. 8), leading to frozen SiO dimers over elemental silicon abundance of less than $\sim 10^{-3}$ in the best case, at low ζ_{CR}. At $\zeta_{CR} \geq 10^{-15}$ s^{-1}, the abundance of SiO dimers over silicon abundance crashes to $\leq 5 \times 10^{-5}$.

We finally note that, in our simulations, we did not include the possibility that CR sputter the ice mantles, which might reduce the mantle size, nor that they could induce reactions among frozen species (e.g. Palumbo & Strazzulla 1993; Dartois et al. 2015).

3.3 The effect of metallicity

Metallicity is likely to play a major role in the composition of the grain mantles. In particular, it may be substantially reduced from the values of the Milky Way in early, high-redshift galaxies. Therefore, we have explored the response of the icy mantle composition to changes in metallicity up to 0.01 of the solar value. We note that for this study we assume that the dust-to-gas ratio scales with metallicity, namely we scaled the abundance of all elements, in the gas and in the dust, by the same amount.

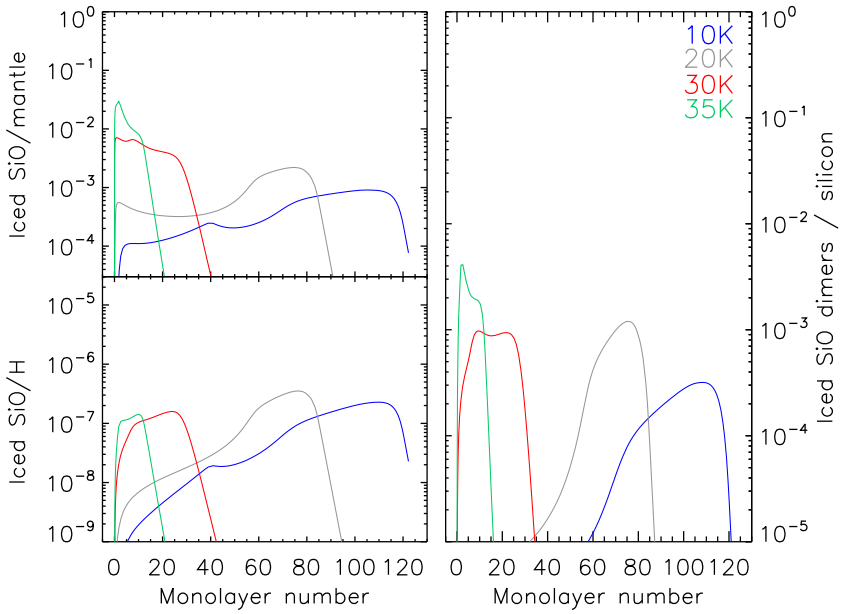

Figure 5. Left-hand panels: iced SiO over the total frozen species of the mantle (top) and iced SiO/H nuclei (bottom) as a function of the monolayers for the four models with different cloud temperatures: 10 K (blue), 20 K (grey), 30 K (red: this is the reference model), and 35 K (green). Right-hand panel: number of iced SiO dimers normalized to the elemental abundance of silicon in the gas phase as a function of the monolayer, for the four models as in the left-hand panels.

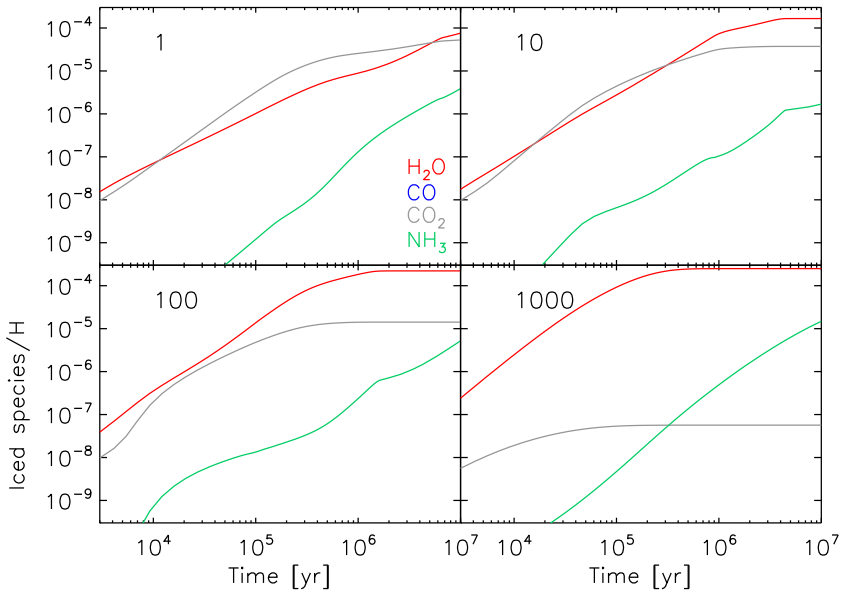

Figure 6. As Fig. 2. The simulations refer to the cases where the CR ionization rate ζ_{CR} is varied with respect to the value 1×10^{-17} s^{-1}: 1 (upper-left panel), 10 (upper-right panel), 100 (bottom-left panel), and 1000 (bottom-right panel) times larger values. The other parameters are those of the reference model (Table 3).

Finally, in order to further reflect the ISM at high redshift, we run a model where the initial elemental abundances are taken from theoretical predictions of the yield from the first generation of massive stars. This is the model Cosmo of Table 2. These yields will depend on the mass of the SN progenitor, and several models lead to critically different values for such abundances (e.g. Chieffi & Limongi 2002; Heger & Woosley 2002; Umeda & Nomoto 2002). For this study, we choose an 80 $M_\odot$ progenitor and use the yields calculated by the Chieffi & Limongi (2002) models. As the yield from SNe will be diluted by mixing with the pristine surrounding gas, we normalize the calculated yields to the carbon abundance of our 0.1 metallicity model, and we assume that half of the carbon and half of the silicon are locked in the grain cores. Assuming that the bulk of the dust is due to carbonaceous grains (see below), we adopted a dust-to-gas ratio equal to 1/300, namely 1/3 the standard one. The initial elemental abundances for this model run are also listed in the last column of Table 2.

The number of layers slightly increases, from 73 to 82, when the metallicity decreases by a factor of 10, but then it drops to 24 layers for a metallicity lower than a factor of 100 with respect to the solar

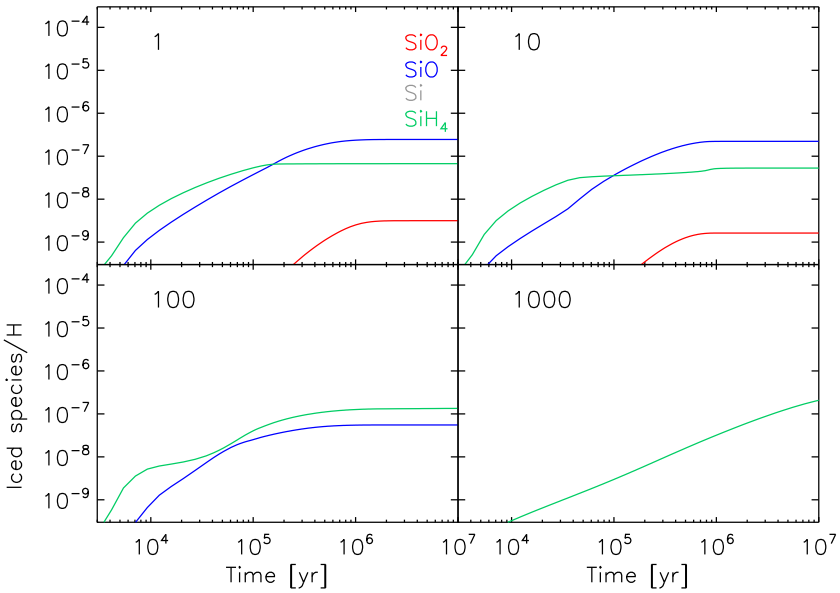

Figure 7. As Fig. 4. The simulations refer to the cases where the CR ionization rate ζ_{CR} is varied with respect to the value 1×10^{-17} s^{-1}: 1 (upper-left panel), 10 (upper-right panel), 100 (bottom-left panel), and 1000 (bottom-right panel) times larger values. The other parameters are those of the reference model (Table 3).

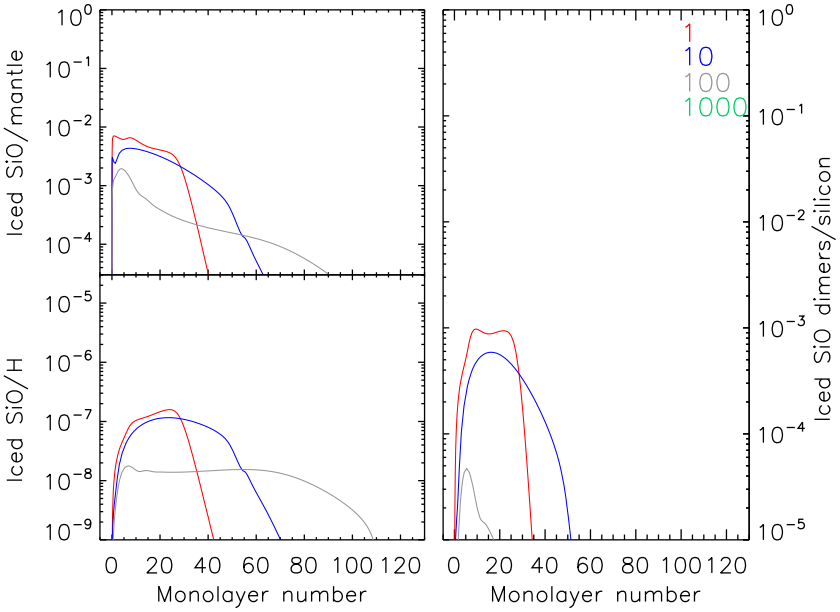

Figure 8. As Fig. 5 for the four models with different CR ionization rate ζ_{CR}: 1 (red), 10 (blue), 100 (grey), and 1000 (green) times 10^{-17} s^{-1}.

one. This is mainly due to the behaviour of the atomic oxygen. With metallicity 0.1 solar, atomic O abundance is always comparable to or less than atomic H, so that water molecules are more easily formed on the surface. However, when the metallicity drops to 0.01, there are too few oxygen atoms. The composition of the mantles is shown in Fig. 9. Water is always the major component, followed by iced CO_2 and ammonia. The Cosmo simulation gives the most different results, which reflect the adopted elementary abundances (Table 2). For example, no ammonia is present because of the very low assumed nitrogen elementary abundance.

In all the simulations with varying metallicity, the abundance of possible SiO dimers is, as in the previous cases, always lower than 10^{-3}, with the exception of the Cosmo simulation, where the gaseous silicon abundance is half of the elemental one. In this case, the dimers' abundance can reach 0.04 the elemental silicon abundance between 20 and 40 monolayers from the bare silicates (Fig. 10). Hence, the Cosmo simulation is the most favourable to the formation of SiO dimers on grains.

3.4 The effect of silicon abundance

One parameter that is certainly crucial in increasing the SiO and SiO_2 abundance in the mantle and, more particularly, in the first layer(s) is the amount of available gaseous silicon. We, therefore, chose to vary the initial elemental abundances of silicon in the gas phase, Si_{gas}, from 1/100 to 90 per cent of the total Si abundance,

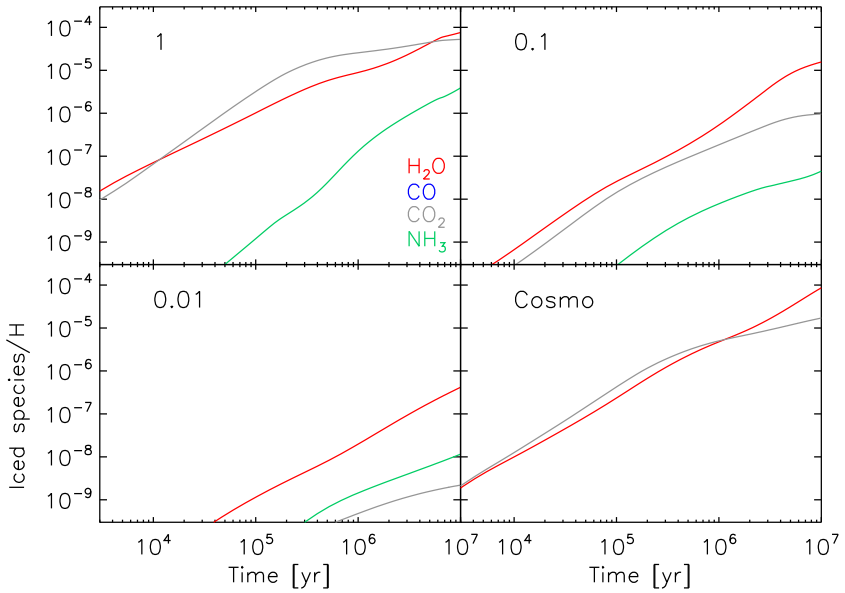

Figure 9. As Fig. 2. The simulations refer to the cases where the metallicity varied with respect to the solar value: 1 (upper-left panel), 0.1 (upper-right panel), 0.01 (bottom-left panel) times larger values, and from cosmic simulations (see the text; bottom-right panel). The other parameters are those of the reference model (Table 3).

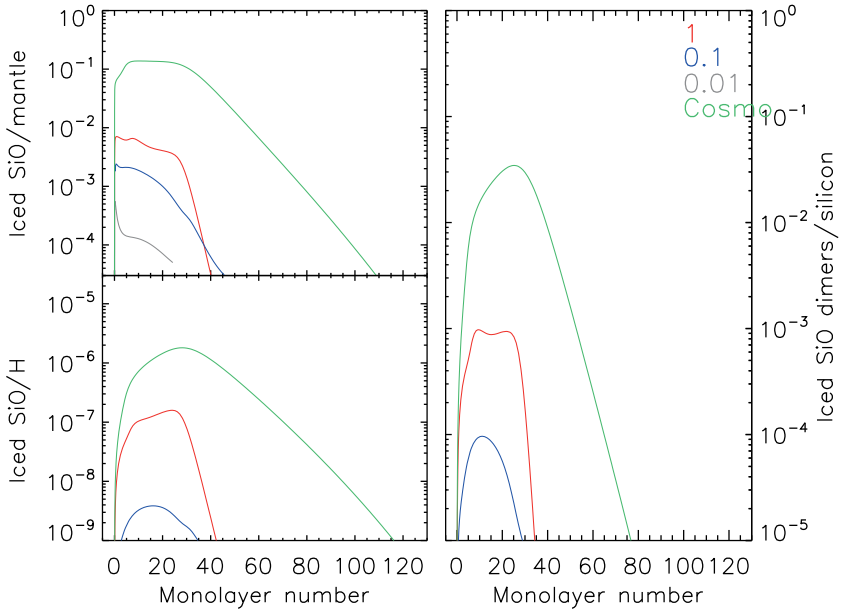

Figure 10. As Fig. 5 for the four models with different metallicities: 1 (red), 0.1 (blue), 0.01 (grey) times the solar value, and from cosmic simulations (see the text; green).

Si_{sol}, assumed to be the solar one (3.2×10^{-5}). If the grain abundance were dominated by the silicates, we should reduce accordingly the dust-to-grain ratio. However, this is not the case even though it is still debated what is the mineralogical nature of the interstellar grains (e.g. Jones et al. 2013). We, therefore, prefer to keep the same dust-to-gas ratio (1/100), with the goal to explore whether any silicate-like (mainly SiO dimers and clusters) could grow on the grain mantles, regardless of the composition of the bare refractory grain.

The results of these simulations are shown in Figs 11 and 12. The number of layers in the mantle increases from 73 ($Si_{gas}/Si_{sol} = 0.01$) to 79 ($Si_{gas}/Si_{sol} = 0.9$) because of gaseous silicon becoming more abundant. Fig. 11 shows the increasing amount of SiO, SiH_4, and SiO_2 with increasing available gaseous silicon (as expected, the curves of iced H_2O and CO_2 do not change). Obviously, increasing the available elemental silicon helps the production of SiO as well as SiO_2 in the ices.

None the less, even with 90 per cent of all the silicon in the gas phase, the iced ratio of SiO never exceeds 0.4 times the other species in the mantle (Fig. 12). The highest value is found in the intermediate layers, between ∼10 and ∼40, where the mantle is dominated by silane first and later by CO_2. However, most importantly, the abundance of SiO dimers with respect to the available elemental silicon never exceeds 0.1 and decreases to 0.01 for Si_{gas}/Si_{sol} equal to 0.1. In other words, even assuming that 90 per cent of silicon is in the gas phase, only 10 per cent of it will perhaps

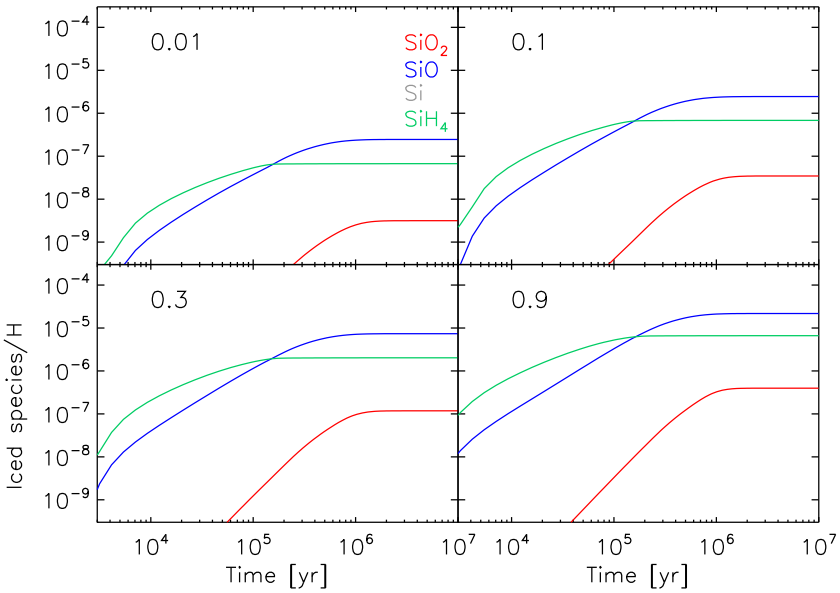

Figure 11. As Fig. 4. The simulations refer to the cases where the gaseous silicon abundance is varied. The Si_{gas}/Si_{sol} is 0.01 (upper-left panel), 0.01 (upper-right panel), 0.3 (bottom-left panel), and 0.9 (bottom-right panel). The other parameters are those of the reference model (Table 3).

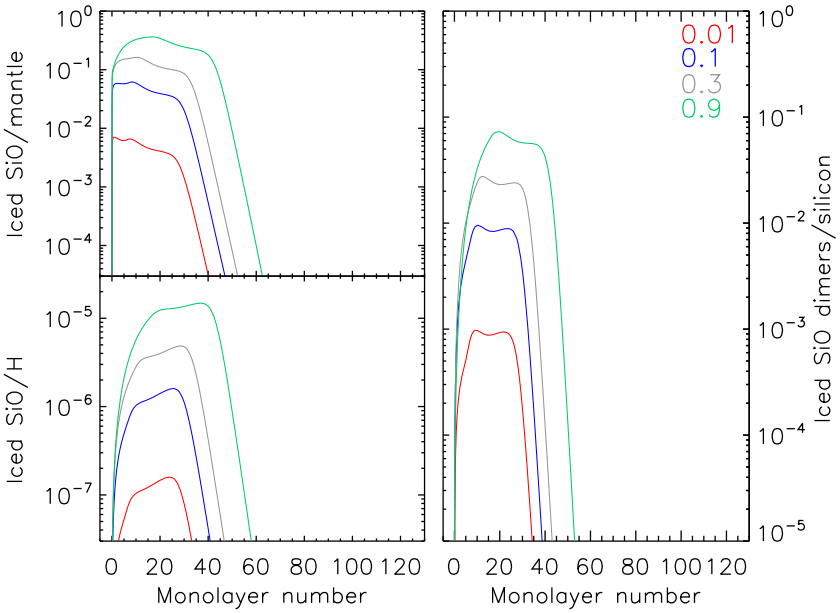

Figure 12. As Fig. 5 for the four models with different Si_{gas}/Si_{sol}: 0.01 (red), 0.1 (blue), 0.3 (grey), and 0.9 (green).

form SiO dimers. Hence, SiO clusters would have extremely low abundances.

4 DISCUSSION

4.1 The composition of grain mantles

The simulations reported in the previous section show that the grain mantle composition is a function of z as well as other parameters such as the CR ionization rate and the metallicity. Table 4 summarizes our results.

Water and carbon dioxide are always the most abundant iced species whereas methane, carbon monoxide, methanol, and formaldehyde are extremely sensitive to the cloud temperature, namely the redshift of the galaxy that the cloud belongs to. Ammonia represents an intermediate case, sensitive to the cloud temperature, the CR ionization rate, and (not surprising) metallicity. Iced silane and SiO are always the major reservoirs of silicon in the grain mantles, whereas atomic silicon and SiO_2 contain a very small fraction, at most a few per cent, of it.

Conversely, the grain iced mantles in distant galaxies might provide crucial information on these different parameters. Perhaps, the most difficult to evaluate by means of observations is the CR ionization rate ζ_{CR}. Our simulations show that the relative abundance of iced water and carbon dioxide might provide this information, with the iced H_2O/CO_2 decreasing with increasing ζ_{CR}. The *James Webb Space Telescope* with its great sensitivity in the NIR, where these two species have ice features, should be able to

Table 4. Summary of the main results of the simulations. The abundances of frozen H_2O, CO, CO_2, NH_3, CH_4, and CH_3OH are in units of 10^{-5} with respect of H nuclei, whereas the abundances of SiO_2, SiO, Si, and SiH_4 are in 10^{-7} units.

Model number	Number of layers	H_2O ($\times10^{-5}$)	CO	CO_2	NH_3	CH_4	CH_3OH	SiO_2 ($\times10^{-7}$)	SiO	Si	SiH_4
CMB temperature											
1	122	8.9	2.1	2.7	2.7	1.3	3.6	0.01	1.3	0.2	1.1
2	117	8.9	1.7	6.2	6.4	1.3	2.8	0.04	1.8	0.00	1.2
3	73	7.6	0.00	5.3	0.4	0.00	0.00	0.03	2.5	0.00	0.7
4	26	2.0	0.00	0.9	0.2	0.00	0.00	0.1	0.3	0.00	0.6
CR ionization rate											
5	73	7.6	0.00	5.3	0.4	0.00	0.00	0.03	2.5	0.00	0.7
6	101	17	0.00	3.7	0.2	0.00	0.00	0.02	2.2	0.00	0.5
7	111	22	0.00	1.4	0.5	0.00	0.00	0.00	0.6	0.00	1.3
8	113	25	0.00	0.00	1.5	0.00	0.00	0.00	0.00	0.00	2.1
Metallicity											
9	73	7.6	0.00	5.3	0.4	0.00	0.00	0.03	2.5	0.00	0.7
10	82	1.6	0.00	0.1	0.04	0.00	0.00	0.00	0.07	0.00	0.07
11	24	0.04	0.00	0.00	0.00	0.00	0.00	0.00	0.00	0.00	0.00
12	141	8.6	0.00	1.7	0.00	0.00	0.00	0.9	27.8	0.00	2.7
Silicon abundance											
13	73	7.6	0.00	5.3	0.4	0.00	0.00	0.03	2.5	0.00	0.7
14	73	7.5	0.00	5.2	0.4	0.00	0.00	0.3	25	0.00	6.8
15	75	7.2	0.00	5.2	0.4	0.00	0.00	1.2	74	0.00	20
16	79	6.5	0.00	5.0	0.4	0.00	0.00	4.0	2.2	0.00	66

constrain ζ_{CR} across the galaxies where the observations are feasible, once the other parameters are known via different observations.

Very few iced H_2O, CO, and CO_2 have been so far detected in external galaxies. Ices have been observed in the Large and Small Magellanic Clouds, LMC and SMC, where, on average, the gas and dust are warmer than in the Galaxy, with dust temperatures around 20–40 K (e.g. van Loon et al. 2010 and references therein) and are metal poorer (e.g. Pagel 2003 and references therein). In the LMC, iced CO_2/H_2O is about twice larger than in the Galaxy (e.g. Shimonishi et al. 2010; Seale et al. 2011), in (rough) agreement with our predictions (Table 4). In SMC, the iced CO_2/H_2O is slightly smaller than in the Galaxy (Oliveira et al. 2013), again in rough agreement with our predictions when also the smaller metallicity is considered. Recent *Akari* observations have revealed the presence of H_2O and CO_2 ices in several nearby star-forming galaxies (Yamagishi et al. 2013, 2015). They find that indeed the ratio of these two species is very region dependent and that it is not easily correlated to a single parameter. In particular, they find that while H_2O ice is detected in all their sample, CO_2 ice is only detected in less than half of the sample and its abundance seems to be correlated with the average dust temperature of the galaxy, in agreement with our predictions.

Clearly, dedicated modelling is needed to better refine the agreement between the observed and predicted iced mantle abundances, which is not the scope of this paper.

One indirect consequence of our simulations is the prediction that interstellar complex organic molecules (iCOMs; Ceccarelli et al. 2017) may be difficult to be synthesized in high-z galaxies. In fact, methanol is believed to be a crucial species for the synthesis of iCOMs (e.g. Garrod & Herbst 2006; Balucani et al. 2015; Taquet, Wirström & Charnley 2016). In the cold molecular clouds of our Galaxy, methanol is mostly synthesized on the grain surfaces via the hydrogenation of CO (e.g. Rimola et al. 2014). However, for z larger than about 4, CO cannot remain frozen on the grain surfaces so that no methanol can be synthesized and, consequently, many of the detected galactic iCOMs might have much smaller abundances. At present, a few iCOMs have been detected in extragalactic sources (e.g. http://www.astro.uni-koeln.de/cdms/molecules), and the most distant galaxy where they were detected is at $z = 0.89$ (Müller et al. 2013). It will be interesting to see whether our model predictions are correct. If they are, planets and comets of high-zeta galaxies might develop a very different organic chemistry with respect to that of the Solar system.

4.2 Can silicate dust grow in high-redshift molecular clouds?

It is clear from the results reported in Section 3 that growing silicate dust is not efficient in any of the parameter space investigated, as the key species, SiO and Si, needed to form dimers and clusters from which a silicate might form are always a very minor iced Si-bearing species. Therefore, our basic conclusion is that only a minor fraction of gaseous silicon can agglomerate into the dust icy mantle to possibly grow silicates. Even in the best case, when 90 per cent of silicon is in the gas phase (Fig. 12), only 10 per cent of it would be able to form SiO dimers. This is just due to the low silicate abundance with respect to oxygen, carbon, and hydrogen, which means that the dust mantles are dominated by O- and C-bearing species.

So far we have not discussed the possibility that carbonaceous grain can grow in molecular clouds. There is now consensus that carbonaceous dust is formed by graphite with different degree of hydrogenation (e.g. Jones et al. 2013). The growth of graphite is even less probable than silicate, as carbon atoms are very rare in the ISM, and in particular in molecular clouds, due to the fact that carbon easily goes from the ionized state to the molecular one (CO), and there is just a small parameter space where it remains atomic (in the so-called photodissociation regions, PDRs). As a matter of fact, it is believed that carbonaceous dust is formed in the AGB and SNe, and that in PDRs it is fragmented and gives rise to the polycyclic aromatic hydrocarbons and the small carbonaceous hydrogenated

grains (Jones et al. 2013, 2017). In this respect, therefore, even the growth of carbonaceous dust seems improbable.

5 CONCLUSIONS

In this paper, we present a theoretical study on the ice mantle evolution as a function of time and physical parameters representative of extragalactic environments at different redshifts. Our aim is twofold: first, we explore how the main ice composition varies with changes in temperatures, CR ionization rates, metallicity, and the amount of silicon in the gas; secondly, we quantify whether grain growth at high redshift can indeed be efficient enough to account for the presumed missing dust mass.

Our main conclusions are the following.

(1) The composition of the iced mantles is a strong function of the redshift of the galaxy that the molecular cloud belongs to. The parameter that affects this composition most is the temperature of the dust, which increases with increasing redshift. While water is always the major mantle component, the relative abundances of CO and CO_2, the other major mantle components in the galactic clouds, strongly depend on the dust temperature, with frozen CO disappearing at $z \geq 4$.

(2) Methanol is unlikely to be abundant in the grain mantles of molecular clouds at redshifts higher than about 4. This also implies that complex organic molecules are unlikely to be abundant in the star-forming regions of those galaxies, with possibly profound implications on the organic chemistry of the nascent planetary systems.

(3) The CR ionization rate ζ_{CR} and metallicity are also extremely important in the final composition of the grain iced mantles. In particular, the frozen H_2O/CO_2 ratio increases with decreasing ζ_{CR}.

(4) Even the most favourable scenario to grain growth, namely ∼90 per cent of the elemental Si in the gas phase and high metallicity, is unlikely to lead to a significant grain growth and, consequently, to any significant contribution towards the presumed missing dust mass problem.

ACKNOWLEDGEMENTS

We warmly thank Raffaella Schneider and Ilse De Looze for insightful discussions on the dust growth in supernova explosions and, in general, in the high-redshift clouds. We acknowledge funding from the European Research Council (ERC) in the framework of the ERC Advanced Grant Project DOC 'The Dawn of Organic Chemistry' GA N. 741002.

REFERENCES

Acharyya K., Herbst E., 2016, ApJ, 822, 105
Asano R. S., Takeuchi T. T., Hirashita H., Inoue A. K., 2013, Earth Planets Space, 65, 213
Balucani N., Ceccarelli C., Taquet V., 2015, MNRAS, 449, L16
Barlow M. J. et al., 2010, A&A, 518, L138
Bayet E., Viti S., Williams D. A., Rawlings J. M. C., Bell T., 2009, ApJ, 696, 1466
Bayet E., Williams D. A., Hartquist T. W., Viti S., 2011, MNRAS, 414, 1583
Bergeron H., Rougeau N., Sidis V., Sizun M., Teillet-Billy D., Aguillon F., 2008, J. Phys. Chem. A, 112, 11921
Bianchi S., Schneider R., 2007, MNRAS, 378, 973
Bisbas T. G., Papadopoulos P. P., Viti S., 2015, ApJ, 803, 37
Boogert A. C. A., Gerakines P. A., Whittet D. C. B., 2015, ARA&A, 53, 541
Ceccarelli C., Hily-Blant P., Montmerle T., Dubus G., Gallant Y., Fiasson A., 2011, ApJ, 740, L4
Ceccarelli C. et al., 2017, ApJ, 850, 176
Chieffi A., Limongi M., 2002, ApJ, 577, 281
Codella C. et al., 2012, ApJ, 774, 164
Dartois E. et al., 2015, A&A, 576, 125
De Looze I., Barlow M. J., Swinyard B. M., Rho J., Gomez H. L., Matsuura M., Wesson R., 2017, MNRAS, 465, 3309
Draine B. T., 2009, in Henning T., Grün E., Steinacker J., eds, ASP Conf. Ser. Vol. 414, Cosmic Dust – Near and Far. Astron. Soc. Pac., San Francisco, p. 453
Dulieu F., Amiaud L., Congiu E., Fillion J.-H., Matar E., Momeni A., Pirronello V., Lemaire J. L., 2010, A&A, 512, A30
Dwek E., Galliano F., Jones A. P., 2007, ApJ, 662, 927
Ferrara A., Viti S., Ceccarelli C., 2016, MNRAS, 463, L112
Garrod R. T., Herbst E., 2006, A&A, 457, 927
Garrod R. T., Wakelam V., Herbst E., 2007, A&A, 467, 1103
Ginolfi M., Graziani L., Schneider R., Marassi S., Valiante R., Dell'Agli F., Ventura P., Hunt L. K., 2018, MNRAS, 473, 4538
Goldsmith P. F., 2001, ApJ, 557, 736
Gong M., Ostriker E. C., Wolfire M. G., 2017, ApJ, 843, 38
Goumans T. P. M., Bromley S. T., 2012, MNRAS, 420, 334
Hasegawa T. I., Herbst E., 1993, MNRAS, 261, 83
He J., Acharyya K., Vidali G., 2016a, ApJ, 823, 56
He J., Acharyya K., Vidali G., 2016b, ApJ, 825, 89
Heger A., Woosley S. E., 2002, ApJ, 567, 532
Hirashita H., Voshchinnikov N. V., 2014, MNRAS, 437, 1636
Hollenbach D., Kaufman M. J., Betgin E. A., Melnick G. J., 2009, ApJ, 690, 149
Hoyle F., Wickramasinghe N. C., 1969, Nature, 223, 459
Jones A. P., Fanciullo L., Köhler M., Verstraete L., Guillet V., Bocchio M., Ysard N., 2013, A&A, 558, A62
Jones A. P., Köhler M., Ysard N., Bocchio M., Verstraete L., 2017, A&A, 602, 46
Kozasa T., Hasegawa H., Nomoto K., 1991, A&A, 249, 474
Krasnokutski S. A., Rouillé G., Jäger C., Huisken F., Zhukovska S., Henning T., 2014, ApJ, 782, 15
Lamberts T., Cuppen H. M., Fedoseev G., Ioppolo S., Chuang K.-J., Linnartz H., 2014, A&A, 570, 57
Loison J. C., Wakelam V., Hickson K. M., Bergeat A., Mereau R., 2014, MNRAS, 437, 930
Mancini M., Schneider R., Graziani L., Valiante R., Dayal P., Maio U., Ciardi B., Hunt L. K., 2015, MNRAS, 451, L70
Martin J. C. G., Blitz M. A., Plane J. M. C., 2009, Phys. Chem. Chem. Phys., 11, 10945
Meijerink R., Spaans M., Loenen A. F., van der Werf P. P., 2011, A&A, 525, 119
Michalowski M. J., Murphy E. J., Hjorth J., Watson D., Gall C., Dunlop J. S., 2010, A&A, 522, A15
Morlino G., 2017, in Marcowith A., Renaud M., Dubner G., Ray A., Bykov A., eds, Proc. IAU Symp. 331, Supernova 1987A: 30 Years Later – Cosmic Rays and Nuclei from Supernovae and Their Aftermaths. Cambridge Univ. Press, Cambridge, p. 230
Müller S. et al., 2013, A&A, 551, 109
Nanni A., Bressan A., Marigo P., Girardi L., 2013, MNRAS, 434, 2390
Oliveira J. M. et al., 2013, MNRAS, 411, L36
Padovani M., Galli D., Glassgold A. E., 2009, A&A, 501, 619
Pagel B. E. J., 2003, in Charbonnel C., Schaerer D., Meynet G., eds, ASP Conf. Ser. Vol. 304, CNO in the Universe. Astron. Soc. Pac., San Francisco, p. 187
Palumbo M.-E., Strazzulla G., 1993, A&A, 269, 568
Rimola A., Taquet V., Ugliengo P., Balucani N., Ceccarelli C., 2014, A&A, 572, 70
Schneider R., Ferrara A., Salvaterra R., 2004, MNRAS, 351, 1379
Seale J. P., Looney L. W., Chen C.-H. R., Chu Y.-H., Gruendl R. A., 2011, ApJ, 727, 36

Shimonishi T., Onaka T., Kato D., Sakon I., Ita Y., Kawamura A., Kaneda H., 2010, A&A, 514, 12
Skouteris D., Vazart F., Ceccarelli C., Balucani N., Puzzarini C., Barone V., 2017, MNRAS, 168, L1
Song L., Kastner J., 2017, ApJ, 850, 118
Sugerman B. E. K. et al., 2006, Science, 313, 196
Taquet V., Ceccarelli C., Kahane C., 2012, A&A, 538, 42
Taquet V., Peters P. S., Kahane C., Ceccarelli C., López-Sepulcre A., Toubin C., Duflot D., Wiesenfeld L., 2013, A&A, 550, 127
Taquet V., Charnley S. B., Sipila O., 2014, ApJ, 791, 1
Taquet V., Wirström E. S., Charnley S. B., 2016, ApJ, 821, 46
Tielens A. G. G. M., 2005, The Physics and Chemistry of the Interstellar Medium. Cambridge Univ. Press, Cambridge
Todini P., Ferrara A., 2001, MNRAS, 325, 726
Umeda H., Nomoto K., 2002, ApJ, 565, 385
Valiante R., Schneider R., Bianchi S., Andersen A. C., 2009, MNRAS, 397, 1661
Valiante R., Schneider R., Salvadori S., Bianchi S., 2011, MNRAS, 416, 1916
van Loon J. T., Oliveira J. M., Gordon K. D., Sloan G. C., Engelbracht C. W., 2010, AJ, 139, 1553
Vaupré S., Hily-Blant P., Ceccarelli C., Dubus G., Gabici S., Montmerle T., 2014, A&A, 568, 50
Ventura P., Dell'Agli F., Schneider R., Di Criscienzo M., Rossi C., La Franca F., Gallerani S., Valiante R., 2014, MNRAS, 439, 977
Wakelam V. et al., 2015, ApJS, 217, 20
Watanabe N., Kouchi A., 2002, ApJ, 571, L173
Yamagishi M., Kaneda H., Ishihara D., Oyabu S., Onaka T., Shimonishi T., Suzuki T., Minh Y. C., 2013, ApJ, 773, L37
Yamagishi M., Kaneda H., Ishihara D., Oyabu S., Onaka T., Shimonishi T., Suzuki T., 2015, ApJ, 807, 29
Zhuvkovska S., Dobbs C., Jenkins E. B., Klessen R. S., 2016, ApJ, 831, 147

This paper has been typeset from a TEX/LATEX file prepared by the author.